J. Cent. South Univ. (2014) 21: 2404−2414
DOI: 10.1007/s11771-014-2194-y

Springer

Cracks coalescence mechanism and cracks propagation paths in rock-like specimens containing pre-existing random cracks under compression

Hadi Haeri[1], Kourosh Shahriar[2], Mohammad Fatehi Marji[3], Parviz Moarefvand[2]

1. Department of Mining Engineering, Science and Research Branch, Islamic Azad University, Tehran, Iran;
2. Department of Mining and Metallurgical Engineering, Amirkabir University of Technology, Tehran, Iran;
3. Mine Exploitation Engineering Department, Faculty of Mining and Metallurgy, Institution of Engineering, Yazd University, Yazd, Iran

Abstract: The mechanism of cracks propagation and cracks coalescence due to compressive loading of the brittle substances containing pre-existing cracks (flaws) was modeled experimentally using specially made rock-like specimens from Portland Pozzolana Cement (PPC). The breakage process of the specimens was studied by inserting single and double flaws with different inclination angles at the center and applying uniaxial compressive stress at both ends of the specimen. The first crack was oriented at 50° from the horizontal direction and kept constant throughout the analysis while the orientation of the second crack was changed. It is experimentally observed that the wing cracks are produced at the first stage of loading and start their propagation toward the direction of uniaxial compressive loading. The secondary cracks may also be produced in form of quasi-coplanar and/or oblique cracks in a stable manner. The secondary cracks may eventually continue their propagation in the direction of maximum principle stress. These experimental works were also simulated numerically by a modified higher order displacement discontinuity method and the cracks propagation and cracks coalescence were studied based on Mode I and Mode II stress intensity factors (SIFs). It is concluded that the wing cracks initiation stresses for the specimens change from 11.3 to 14.1 MPa in the case of numerical simulations and from 7.3 to 13.8 MPa in the case of experimental works. It is observed that cracks coalescence stresses change from 21.8 to 25.3 MPa and from 19.5 to 21.8 MPa in the numerical and experimental analyses, respectively. Comparing some of the numerical and experimental results with those recently cited in the literature validates the results obtained by the proposed study. Finally, a numerical simulation was accomplished to study the effect of confining pressure on the crack propagation process, showing that the SIFs increase and the crack initiation angles change in this case.

Key words: crack propagation; crack coalescence; rock-like specimen; numerical simulation; experiment

1 Introduction

Experimental works are mainly used to study the crack propagation and crack coalescence phenomena in brittle substances such as rocks [1−5]. The pre-existing cracks in rocks are normally under compressive loading and mainly propagate in a stable manner due to formation of wing and/or secondary cracks [6]. It is mainly expected that the crack initiation will follow in the direction (approximately) parallel to the maximum compressive stress [7−9]. In a crack propagation process of the brittle substances such as rock-like specimens, usually two types of cracks are observed originating from the original tips of pre-existing cracks (i.e. wing cracks and secondary cracks as shown in Fig. 1). Wing cracks are usually produced due to tension while secondary cracks may initiate due to shear. Therefore, initiation of wing cracks in rocks is favored relative to secondary cracks because of the lower toughness of these materials in tension than in shear [10].

Wing cracks are usually considered as the emanating tensile cracks that initiate at or near the original tips of pre-existing cracks and propagate in a curved path (with increasing load) and the secondary cracks may be considered as shear cracks that may grow from the original tips of the flaws. Secondary cracks may initiate in two different directions, coplanar (quasi-coplanar) and oblique to the pre-existing cracks [11−12].

Many experimental works have been devoted to study the crack initiation, propagation, interaction and eventual coalescence of the pre-existing cracks in specimens of various substances, including natural rocks or rock-like materials under compressive loading [13−26].

Recently, PARK and BOBET [27] carried out compression tests on prismatic gypsum specimens with

Received date: 2013−09−22; **Accepted date:** 2013−12−31
Corresponding author: Hadi Haeri, PhD Candidate; E-mail: haerihadi@ymail.com, hadihaeri@ymail.com

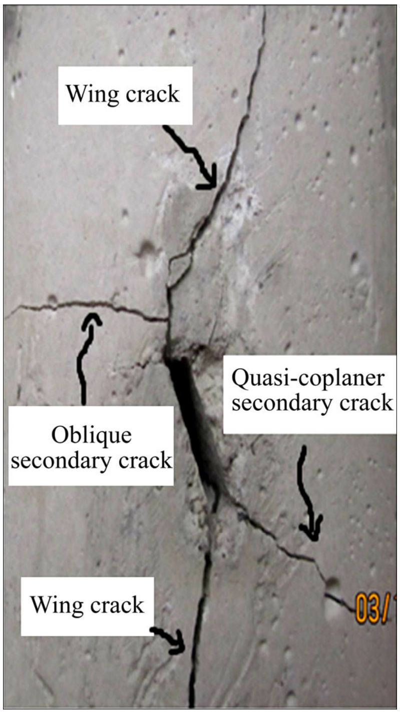

Fig. 1 A propagated center slant flaw under uniaxial compression

three closed flaws and compared the cracking process in specimens with open flaws. The differences between open and closed flaws with different geometries are investigated. Seven types of cracks coalescence were observed in their experimental works. LEE and JEON [28] experimentally studied the propagation process of single and double flaws in PMMA (poly methyl meth acrylate), diastone, and Hwangdeung granite specimens. PU and CAO [29] conducted compression tests on rock-like specimens with closed multi-fissures and investigated the influence of fissure inclination angle and distribution density on the breakage characteristics of fissured bodies.

Various numerical methods have been developed for the simulation of crack propagation in brittle substances, e.g. finite element method (FEM), boundary element method (BEM), and discrete element method (DEM).

Three important breakage initiation criteria were proposed to study the crack propagation mechanism of brittle materials: 1) the maximum tangential stress (σ_θ-criterion) [30], 2) the maximum energy release rate (G-criterion) [31] and 3) the minimum energy density criterion (S-criterion) [32]. Some modified form of the mentioned criteria e.g. F-criterion which is a modified energy release rate criterion proposed by SHEN and STEPHANSSON [33] may also be used to study the breakage behavior of brittle substances [34−35]. Several computer codes were used to model the breakage mechanism in brittle materials such as rocks, i.e. FROCK code [24], rock failure process analysis (RFPA^{2D}) code [36], and 2D particle flow code (PFC^{2D}) [28, 37].

The experimental works on rock-like specimens containing single and double flaws with different inclinations have been accomplished to study the cracks propagation and cracks coalescence phenomena in rock-like specimens (specimens are prepared mainly form PCC, fine sand and water). Some of the experimental works are simulated numerically by a modified higher order displacement discontinuity code and the cracks propagation and cracks coalescence paths are studied based on Mode I and Mode II stress intensity factors. The experimental results are compared with the numerical results which confirm each other and illustrate the accuracy and validity of the proposed work. The numerical simulation can insert the required flexibility in the present analyses so that it may be readily possible to investigate the effect of confining pressure on the wing crack initiation angles and their Mode I and Mode II stress intensity factors.

2 Specimen preparation and testing

In the present work, rock-like specimens are made basically from Portland Pozzolana Cement (PPC). PPC, fine sand and water are mixed in suitable ratios for preparing rock-like specimens with 60 mm in diameter and 120 mm in length (Fig. 2).

Table 1 gives the mechanical properties of the rock-like specimens obtained from the laboratory tests.

Various uniaxial compression tests are conducted on rock-like specimens containing two random Flaws 1 and 2 (Fig. 3(a)). The inclination angle, α of Flaw 1 is kept constant (α=50°) but Flaw 2 may experience variable inclination angles, φ=0°, 30°, 60° and 90°.

Fig. 2 Typical rock-like specimens prepared for laboratory test

Table 1 Mechanical properties of rock-like specimens

Parameter	Value
Uniaxial compression strength, σ/MPa	26
Elastic modulus, E/GPa	17
Poisson ratio, ν	0.21
Fracture toughness, K_{IC}/(MPa·m$^{1/2}$)	2

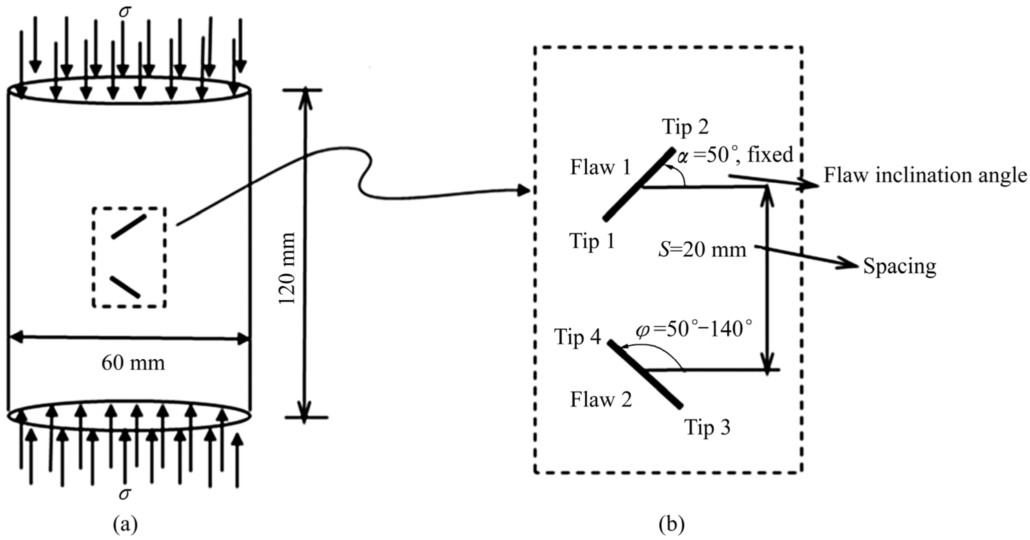

Fig. 3 Geometry of two random flaws in a rock-like specimen under uniaxial compression

These flaws are created by inserting two thin steel shims with 10 mm in width and 1 mm in thickness in the mold (before casting the specimens). The uniaxial compressive stress, σ, was uniformly applied and the loading rate was kept at 0.2 MPa/s during the tests.

Figure 3(b) demonstrates a schematic view of the geometry of two random flaws (i.e. Flaw 1 and Flaw 2) with equal length $2b$=10 mm. The locations of flaws are also determined by positions of the flaw tips i.e. Tip 1, Tip 2, Tip 3 and Tip 4, respectively.

Therefore, four specimens are prepared each containing two random flaws, 1 and 2, as shown in Fig. 4.

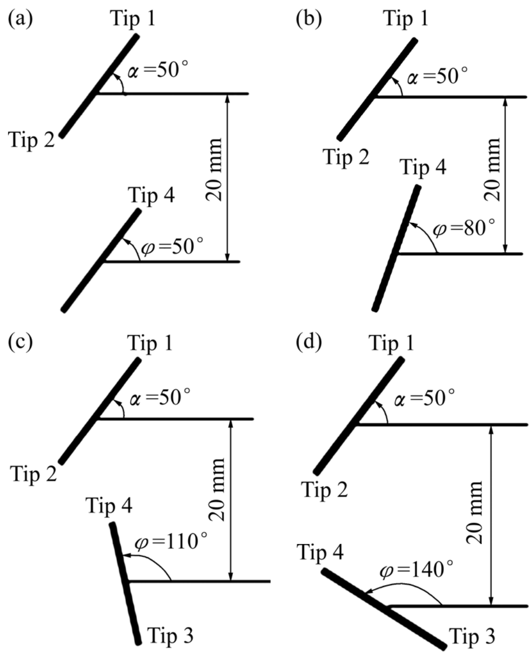

Fig. 4 Flaw geometries with spacing S=20 mm: (a) α=50°, φ=50°; (b) α=50°, φ=80°; (c) α=50°, φ=110°; (d) α=50°, φ=140°

2.1 Production of wing and secondary cracks considering a single flaw (Flaw 1)

Some experimental works have been accomplished to study the mechanism of initiation and propagation of wing and secondary cracks emanating from a single 50° center slant flaw. Figure 5 illustrates the production of wing and secondary cracks originating from the tips of the pre-existing center slant crack. The propagation paths are curved and the wing and secondary cracks propagate towards the direction of the uniaxial compressive stress applied to the specimen during the experiment. As the load increases, the wing cracks propagate further and their aperture increases. The secondary cracks are usually stable cracks propagating after the wing cracks and may

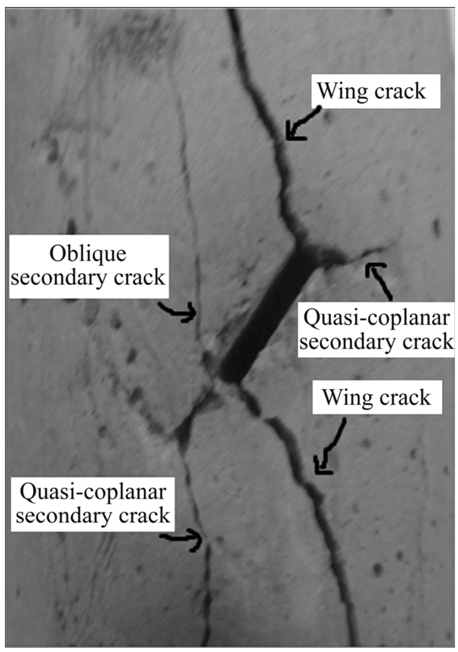

Fig. 5 Cracking pattern in rock-like specimen considering a single flaw (Flaw 1)

be divided into two main types: 1) quasi-coplanar secondary cracks propagating in the plane of the original flaw, and 2) oblique secondary cracks propagating in the plane of wing cracks, i.e. nearly perpendicular to the direction of the original flaw.

2.2 Crack coalescence of rock-like specimens containing two flaws

Cracks coalescence phenomenon occurs when the two pre-existing cracks combine due to propagation of wings and/or secondary cracks (originating from the tips of the pre-existing cracks) in brittle substances under various loadings.

In the current experimental works, the wing cracks are instantaneously initiated quasi-statically (Fig. 6). The development and coalescence of wing cracks may be the main cause of the breakage paths in rock-like specimens. Then the secondary cracks may be developed and coalesced with the wing cracks in a stable manner. As illustrated in Fig. 6, the experimental tests demonstrate that the secondary cracks may not always be observed, but the wing cracks appear instantaneously. Wing cracks may start their initiation at stress levels of about one half that of the specimen's strength, otherwise, the secondary cracks may approximately occur near the peak strength of the specimens and extend unstably after the wing cracks propagation. Figures 6(a)−(d) show the observed wing cracks propagating toward each other and causing crack coalescence.

Figures 6 (a)−(b) illustrate four cases of coalescence paths due to the propagation of the wing cracks that are observed in the experiments.

3 Numerical method

A displacement based version of the indirect boundary element method known as displacement discontinuity method (DDM) originally proposed by CROUCH [38] for the solution of elastostatic problems in solid mechanics is used in this work [39−44].

In this research, a higher accuracy of the displacement discontinuities along the boundary of the problem is obtained by using quadratic displacement discontinuity (DD) elements. A quadratic DD element is divided into three equal sub-elements where each sub-element contains a central node for which the nodal DD is evaluated numerically [34−35].

Figure 7 shows the displacement distribution at

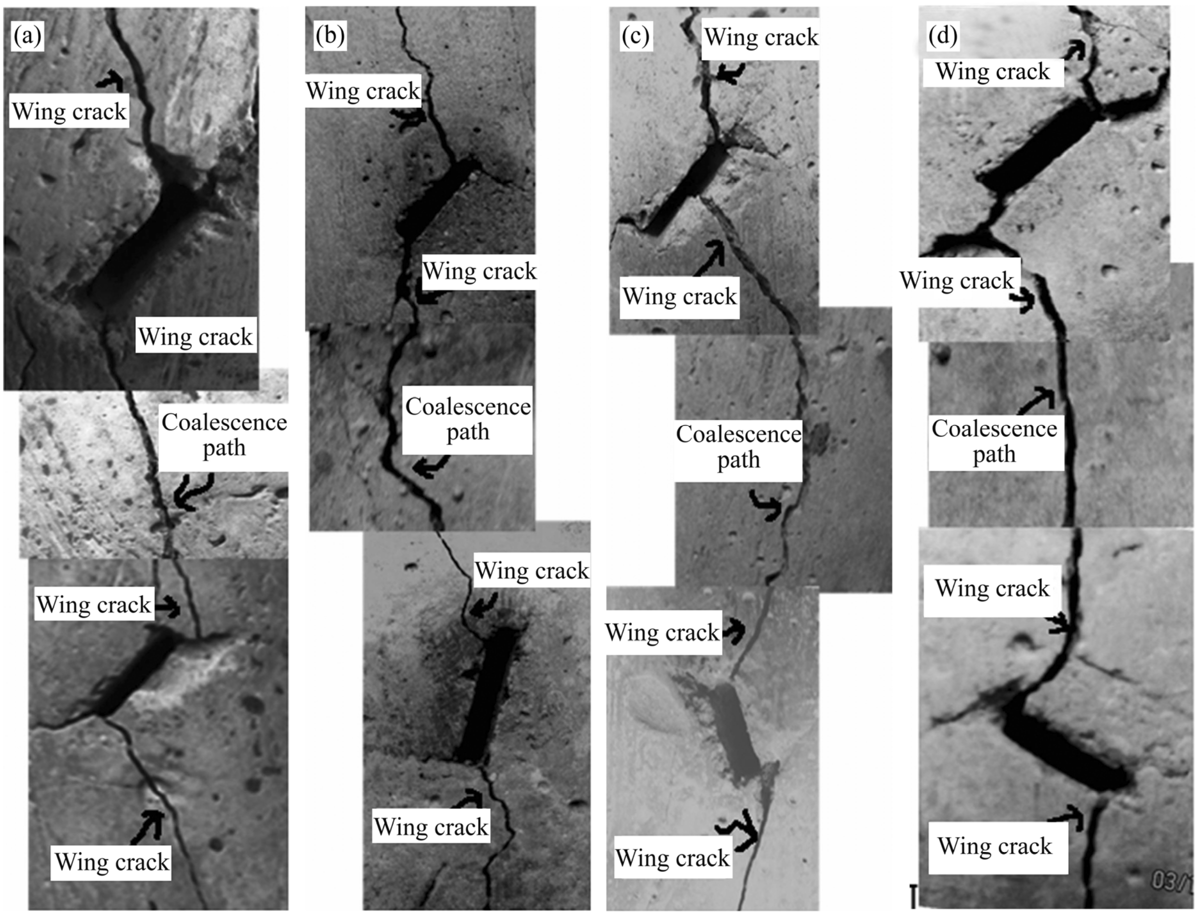

Fig. 6 Experimental results illustrating coalescence path of rock-like specimens containing two flaws: (a) α=50°, φ=50°; (b) α=50°, φ=80°; (c) α=50°, φ=110°; (d) α=50°, φ=140°

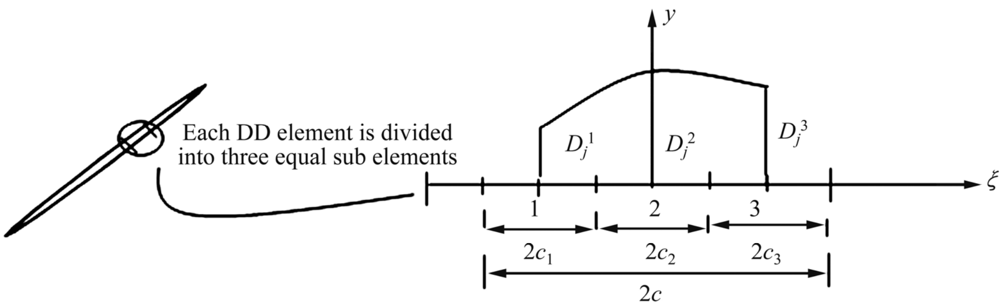

Fig. 7 Quadratic collocations for higher order displacement discontinuity variation

quadratic collocation point m, which can be calculated as

$$D_j(\zeta)=\sum A_m(\zeta)D_j^m\ (j=x,y;\ m=1,2,3) \tag{1}$$

where D_j^1, D_j^2 and D_j^3 are the quadratic nodal displacement discontinuities (DDs) in x and y directions. Considering a quadratic element of length, $2c$, with equal sub-elements ($c_1=c_2=c_3$) and a quadratic shape function, $A_m(\zeta)$ for $-c\le\zeta\le c$, the following shape functions of the quadratic collocation point m can be defined as [34]

$$\begin{cases}A_1(\varepsilon)=\zeta(\zeta-2c_1)/8{c_1}^2\\ A_2(\zeta)=-(\zeta^2-4{c_1}^2)/4{c_1}^2\\ A_3(\zeta)=\zeta(\zeta+2c_1)/8{c_1}^2\end{cases} \tag{2}$$

The stresses and displacements for an oriented straight flaw in an infinite specimen along x-axis, in terms of single harmonic functions $f(y, x)$ and $g(y, x)$, are given by CROUCH and STARFIELD [45] as

$$\begin{cases}\sigma_{xx}=2\rho[2f_{,xy}+yf_{,xyy}]+2\rho[g_{,yy}+yg_{,yyy}]\\ \sigma_{yy}=2\rho[-yf_{,xyy}]+2\rho[g_{,yy}-yg_{,yyy}]\\ \sigma_{xy}=2\rho[2f_{,yy}+yf_{,yyy}]+2\rho[-yg_{,xyy}]\end{cases} \tag{3}$$

And the displacements are

$$\begin{cases}u_x=[2(1-\nu)f_{,y}-yf_{,xx}]+[-(1-2\nu)g_{,x}-yg_{.xy}]\\ u_y=[(1-2\nu)f_{,x}-yf_{,xy}]+[2(1-\nu)g_{,y}-yg_{.yy}]\end{cases} \tag{4}$$

where ρ is shear modulus and f_y, g_y, f_x, g_x, etc are the partial derivatives of the single harmonic functions $f(y, x)$ and $g(y, x)$ with respect to y and x. These potential functions (for a quadratic variation of DD along the element) can be written as

$$\begin{cases}f(x,y)=\dfrac{-1}{4\pi(1-\nu)}\displaystyle\sum_{m=1}^{3}D_x^m\varOmega_m(I_0,I_1,I_2)\\ g(x,y)=\dfrac{-1}{4\pi(1-\nu)}\displaystyle\sum_{m=1}^{3}D_y^m\varOmega_m(I_0,I_1,I_2)\end{cases} \tag{5}$$

The common function, $\varOmega_m$, can be defined as

$$\varOmega_m(I_0,I_1,I_2)=\int A_m(\zeta)\ln[(x-\zeta)+y^2]^{\frac{1}{2}}\mathrm{d}\zeta\ (m=1,2,3) \tag{6}$$

The integrals I_0, I_1 and I_2 in Eq. (6) can be obtained as

$$\begin{aligned}I_0(x,y)&=\int_{-c}^{c}\ln[(x-\zeta)^2+y^2]^{1/2}\mathrm{d}\zeta\\ &=y(\psi_1-\psi_2)-(x-c)\ln\varGamma_1+(x+c)\ln\varGamma_2-2c\end{aligned} \tag{7a}$$

$$\begin{aligned}I_1(x,y)&=\int_{-c}^{c}\zeta\ln[(x-\zeta)^2+y^2]^{1/2}\mathrm{d}\zeta\\ &=xy(\psi_1-\psi_2)+0.5(y^2-x^2+c^2)\ln(\varGamma_1/\varGamma_2)-cx\end{aligned} \tag{7b}$$

$$\begin{aligned}I_2(x,y)&=\int_{-c}^{c}\zeta^2\ln[(x-\zeta)^2+y^2]^{1/2}\mathrm{d}\zeta\\ &=y/3(3x^2-y^2)(\psi_1-\psi_2)+1/3(3xy^2-x^3+\\ &\quad c^3)\ln\varGamma_1-1/3(3xy^2-x^3-c^3)\ln\varGamma_2-\\ &\quad 2c/3(x^2-y^2+c^2/3)\end{aligned} \tag{7c}$$

where ψ_1, ψ_2, $\varGamma_1$ and $\varGamma_2$ can be derived as

$$\begin{cases}\psi_1=\arctan(\dfrac{y}{x-c})\\ \psi_2=\arctan(\dfrac{y}{x+c})\\ \varGamma_1=[(x-c)^2+y^2]^{1/2}\\ \varGamma_2=[(x+c)^2+y^2]^{1/2}\end{cases} \tag{8}$$

To eliminate the singularity of the displacements and stress calculation near the flaw ends and increase the accuracy of higher order displacement discontinuity method around the original flaw tip, a special treatment of the flaw at the tip is necessary [46−47]. In previous works, usually, one or two elements for specific flaw tip were used, but in the present research three special flaw tip elements at the flaw ends are used in the general higher order displacement discontinuity method. As shown in Fig. 8, the DD variation for three nodes can be formulated using a special flaw tip element containing three nodes (or having three special flaw tip sub-elements) [34]:

$$D_j(\zeta)=\sum A_{\mathrm{T}m}(\zeta)D_j^m(c)(j=x,y;\ m=1,2,3) \tag{9}$$

Considering a flaw tip element with the three equal sub-elements ($c_1=c_2=c_3$), the shape functions $A_{\mathrm{T}1}(\zeta)$, $A_{\mathrm{T}2}(\zeta)$ and $A_{\mathrm{T}3}(\zeta)$ can be obtained as

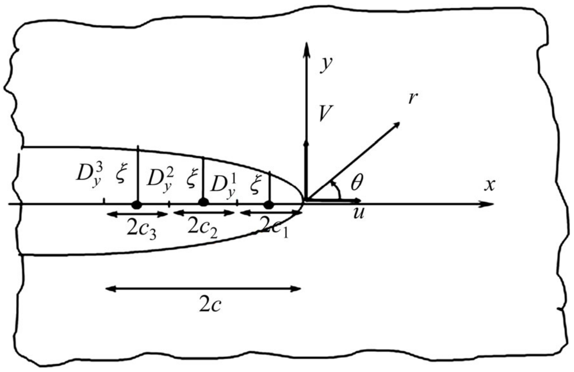

Fig. 8 A special flaw tip element with three equal sub-elements

$$\begin{cases} A_{\mathrm{T1}}(\zeta)=\dfrac{15\zeta^{1/2}}{8c_1^{1/2}}-\dfrac{\zeta^{3/2}}{c_1^{3/2}}+\dfrac{\zeta^{5/2}}{8c_1^{5/2}} \\ A_{\mathrm{T2}}(\zeta)=\dfrac{-5\zeta^{1/2}}{4\sqrt{3}c_1^{1/2}}+\dfrac{3\zeta^{3/2}}{2\sqrt{3}c_1^{3/2}}-\dfrac{\zeta^{5/2}}{4\sqrt{3}c_1^{5/2}} \\ A_{\mathrm{T3}}(\zeta)=\dfrac{3\zeta^{1/2}}{8\sqrt{5}c_1^{1/2}}-\dfrac{\zeta^{3/2}}{2\sqrt{5}c_1^{3/2}}+\dfrac{\zeta^{5/2}}{8\sqrt{5}c_1^{5/2}} \end{cases} \tag{10}$$

The common function $\Omega_{\mathrm{T}}^m(I_{\mathrm{T}}^1, I_{\mathrm{T}}^2, I_{\mathrm{T}}^3)$ is defined as

$$\Omega_{\mathrm{T}}^m(I_{\mathrm{T}}^m)=\int_{-c}^{c}A_{\mathrm{T}m}(\zeta)\ln[(x-\zeta)^2+y^2]^{1/2}\mathrm{d}\zeta \quad (m=1,\ 2,\ 3) \tag{11}$$

The integrals I_{T}^1, I_{T}^2 and I_{T}^1 can be expressed as

$$\begin{cases} I_{\mathrm{T}}^1(x,y)=\int_{-c}^{c}\zeta^{1/2}\ln[(x-\zeta)^2+y^2]^{1/2}\mathrm{d}\zeta \\ I_{\mathrm{T}}^2(x,y)=\int_{-c}^{c}\zeta^{3/2}\ln[(x-\zeta)^2+y^2]^{1/2}\mathrm{d}\zeta \\ I_{\mathrm{T}}^3(x,y)=\int_{-c}^{c}\zeta^{5/2}\ln[(x-\zeta)^2+y^2]^{1/2}\mathrm{d}\zeta \end{cases} \tag{12}$$

The mode I and mode II stress intensity factors K_{I} and K_{II} can be estimated based on LEFM theory as the opening and sliding displacements [48]:

$$\begin{cases} K_{\mathrm{I}}=\dfrac{\rho}{4(1-\nu)}\left(\dfrac{2\pi}{c}\right)^{1/2}D_y(c) \\ K_{\mathrm{II}}=\dfrac{\rho}{4(1-\nu)}\left(\dfrac{2\pi}{c}\right)^{1/2}D_x(c) \end{cases} \tag{13}$$

3.1 Numerical simulation of experimental works

A modified higher order displacement discontinuity method based on the versatile boundary element method [49] is used for the numerical simulation of the experimental works proposed in this work to study the cracks coalescence and cracks propagation process of brittle substances under compressive loading conditions. The four different specimens already shown in Figs. 6(a)−(d) are simulated numerically by the proposed numerical method and the results are shown graphically in Figs. 9(a)−(d). The linear elastic fracture mechanics (LEFM) approach based on the concept of SIFs proposed by IRWIN [50] is implemented in the boundary element code and the maximum tangential stress criterion given by ERDOGAN and SIH [30] are used in a stepwise procedure to estimate the propagation path of the propagating wing cracks. An iterative method explained by MARJI and DEHGHANI [51] has been used to investigate the crack propagation directions and paths after each crack extension step, Δb=0.1b, successively. The crack propagation paths of each flaw have been estimated by this iterative method and finally the coalescence of the cracks has been observed (after the propagation of wing cracks). As it is quite clear from the results shown in Fig. 9, the numerically simulated propagation paths are in good agreement with the corresponding experimentally observed paths (already shown in Fig. 6).

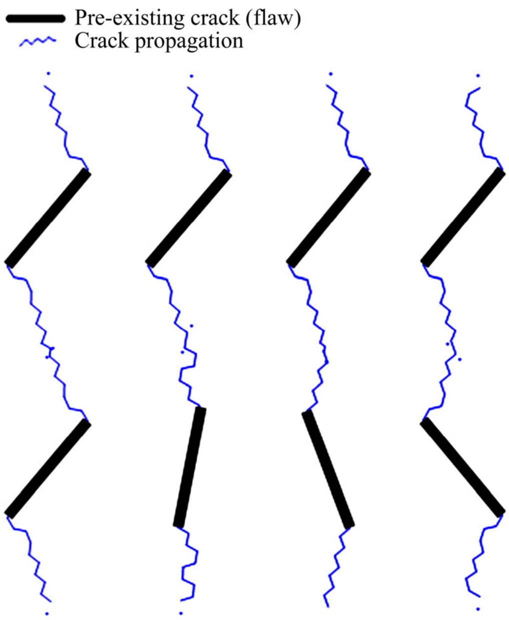

Fig. 9 Numerical simulation of crack coalescence path for specimens containing two flaws: (a) α=50°, φ=50; (b) α=50°, φ=80°; (c) α=50°, φ=110°; (d) α=50°, φ=140°

Figure 10 compares the numerical and experimental results by considering the cracks initiation and cracks coalescence stresses. It has been observed that the wing cracks initiation stresses for various samples change from 11.3 to 14.1 MPa in the case of numerical analysis and from 7.3 to 13.8 MPa in the case of experimental works. On the other hand, the cracks coalescence stresses change from 21.8 to 25.3 MPa for the numerical analysis and from 19.5 to 21.8 MPa for the experimental analysis.

3.2 Effects of orientation and randomness of flaws on their SIF

The mode I stress intensity, K_{I} and mode II stress

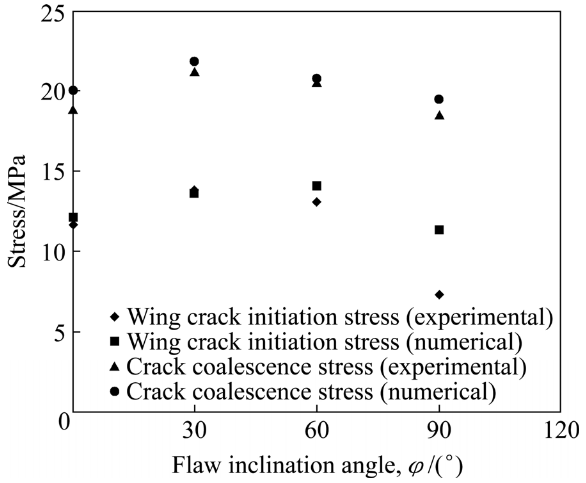

Fig. 10 Comparison of wing crack initiation and cracks coalescence stresses (using numerical simulation and experiments works)

intensity factor, $K_{\rm II}$, are normalized as

$$\begin{cases} K_{\rm I}^{\rm N}=\dfrac{K_{\rm I}}{\sigma\sqrt{\pi b}} \\ K_{\rm II}^{\rm N}=\dfrac{K_{\rm II}}{\sigma\sqrt{\pi b}} \end{cases} \tag{14}$$

The values of the normalized SIFs, $K_{\rm I}$ and $K_{\rm II}$, near the original tips of two random flaws are estimated by considering Flaw 1 with a constant inclination angle, α=50° and Flaw 2 with different inclination angles, φ= 50°, 60°, 70°, 80°, 90°, 100°, 110°, 120°, 130° and 140°. The values of $K_{\rm I}^{\rm N}$, $K_{\rm II}^{\rm N}$ and θ are obtained for the first step of crack propagation process. Table 2 presents the values of $K_{\rm I}^{\rm N}$, and $K_{\rm II}^{\rm N}$ at each of the four tips of the two flaws.

To demonstrate the effect of the second flaw (Flaw 2) on the cracks coalescence and cracks propagation paths, the numerical values of $K_{\rm I}^{\rm N}$, and $K_{\rm II}^{\rm N}$ for the first flaw (Flaw 1) in the absence of the second flaw (Flaw 2) i.e. for a single flaw, are also shown in Figs. 11 and 12, respectively.

The numerical results demonstrate that the final crack propagation paths are strongly depended on the inclination of the second flaw (Flaw 2) as shown in Table 2 and Figs. 11 and 12.

As shown in Fig. 11, $K_{\rm I}^{\rm N}$ has a maximum value at φ=80° for the flaw Tip 1 and there may be no interaction at $\varphi\approx 50^\circ$ and $\varphi\approx 95^\circ$. For the flaw Tip 2, the value of $K_{\rm I}^{\rm N}$ may decrease when the two flaws (Flaw 1 and Flaw 2) overlap slightly whereas, and $K_{\rm I}^{\rm N}$ may increase when two flaws overlap considerably.

According to Fig. 12, the behavior of $K_{\rm II}^{\rm N}$ is usually different from that of $K_{\rm I}^{\rm N}$. For the flaw Tip 1, $K_{\rm II}^{\rm N}$ has a maximum value at $\varphi\approx 90^\circ$ which is close to the value of $K_{\rm II}^{\rm N}$ for a single flaw. In addition, there is a little change in the value of $K_{\rm II}^{\rm N}$ for the flaw Tip 2 when φ changes between 70° and 100°. It may be concluded that for the closer flaw tips, the values of $K_{\rm I}^{\rm N}$ and $K_{\rm II}^{\rm N}$ increase and tend towards the values estimated for a single flaw.

3.3 Effect of confining pressure

Since the experimental analysis of the crack propagation process of rock-like specimens is somewhat time-consuming, expensive, difficult and complex, the numerical simulations of crack propagation process are also accomplished by the indirect boundary element method. As experimentally shown in the previous section, the flaw inclination angle in double-flawed specimens has a significant effect on the coalescence process of the two pre-existing cracks. In this work, the effect of confining pressure on the crack propagation process has been investigated considering single-flawed specimens with different flaw inclination angles under biaxial compressive loading. To do this, consider a rock specimen with length L=120 mm and width w=60 mm

Table 2 Numerical values of $K_{\rm I}^{\rm N}$ and $K_{\rm II}^{\rm N}$ for tips of two pre-existing cracks

Flaw inclination angle		$K_{\rm I}^{\rm N}$				$K_{\rm II}^{\rm N}$			
α/(°)	φ/(°)	Tip 1	Tip 2	Tip 3	Tip 4	Tip 1	Tip 2	Tip 3	Tip 4
50	50	0.4195	0.4372	0.6367	0.6157	0.463	0.4838	0.3981	0.2196
50	60	0.4233	0.4342	0.2732	0.2658	0.4766	0.4915	0.4318	0.4144
50	70	0.4273	0.4323	0.1398	0.1402	0.4863	0.4966	0.3260	0.3129
50	80	0.4275	0.4285	0.0489	0.0554	0.4941	0.4992	0.1808	0.1773
50	90	0.4236	0.4233	0.0143	0.0203	0.4985	0.4990	0.0142	0.0210
50	100	0.4208	0.4217	0.3930	0.0451	0.4962	0.4964	0.1524	0.0941
50	110	0.4064	0.4122	0.1216	0.1130	0.4934	0.4905	0.3035	0.2881
50	120	0.3966	0.4082	0.2487	0.2344	0.4847	0.4836	0.4157	0.4054
50	130	0.3873	0.4051	0.6052	0.5867	0.4718	0.474	0.3979	0.2395
50	140	0.3825	0.4053	0.5788	0.5667	0.4631	0.4699	0.4792	0.4742

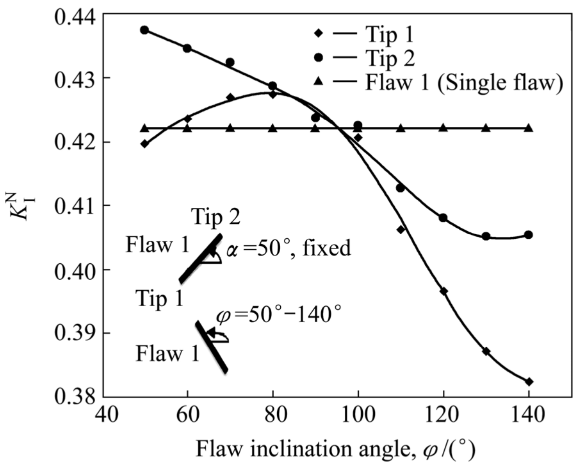

Fig. 11 Treatment of K_I^N versus changes of flaw inclination angle (φ)

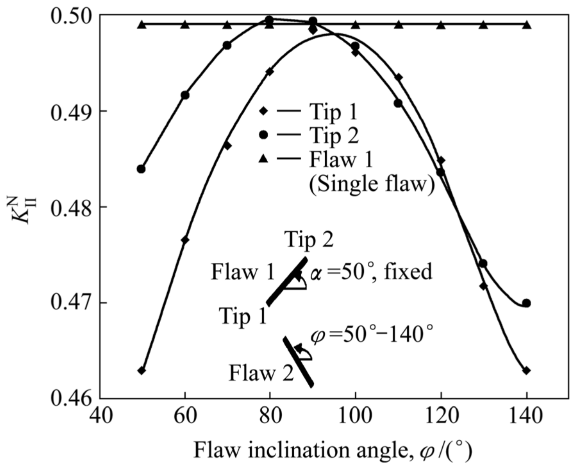

Fig. 12 Treatment of K_{II}^N versus changes of flaw inclination angle (φ)

(L/w=2) containing a center slant flaw with a half-length, b=5 mm, as schematically shown in Fig. 13. The mechanical properties of this finite specimen are the same as those already given in Table 1.

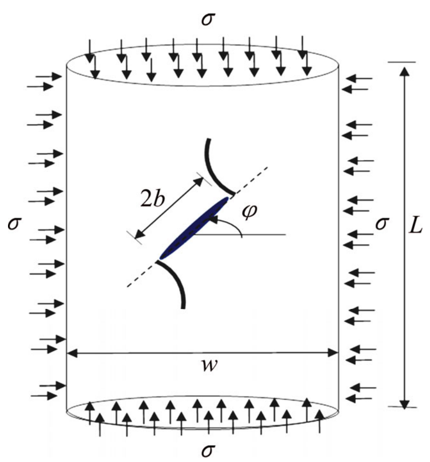

Fig. 13 A schematic view of a propagated center slant flaw (with two wing cracks) in a rock specimen under biaxial compression

Several single-flawed specimens under biaxial compressive loading are simulated to study the effect of the flaw inclination angle on the wing crack initiation angle and normalized SIFs by the higher order displacement discontinuity method.

The numerical results of wing crack initiation angles and normalized SIFs in specimens containing single flaw with varying inclination angles, φ=0°, 15°, 30°, 45°, 60° and 75° under the confinement of 0, 5 and 10 MPa are shown in Figs. 14−16. As shown in Fig. 14, the confining pressure strengthens the material and causes the wing crack initiation angles to be diverted from the direction of the maximum (vertical) stress (10 MPa) and finally they may produce a shear like fracture plane as is usually expected from the results of the conventional biaxial compression tests carried out on the intact rock specimens.

According to Figs. 15 and 16, increasing the confinement stress causes increasing of K_I^N and K_{II}^N for all flaw inclination angles.

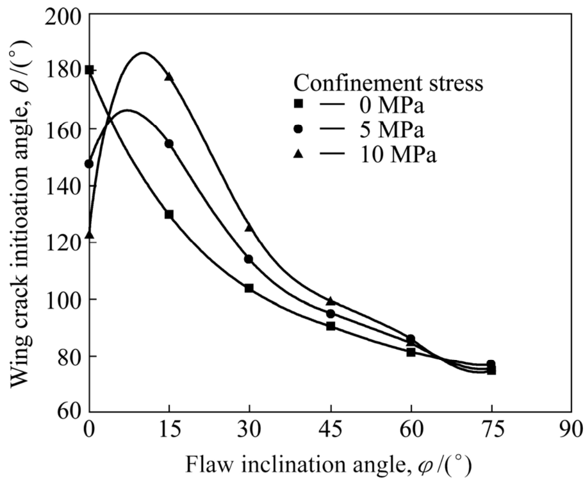

Fig. 14 Variation of wing crack initiation angles versus changes of flaw inclination angles (φ) for confinement stress of 0, 5 and 10 MPa

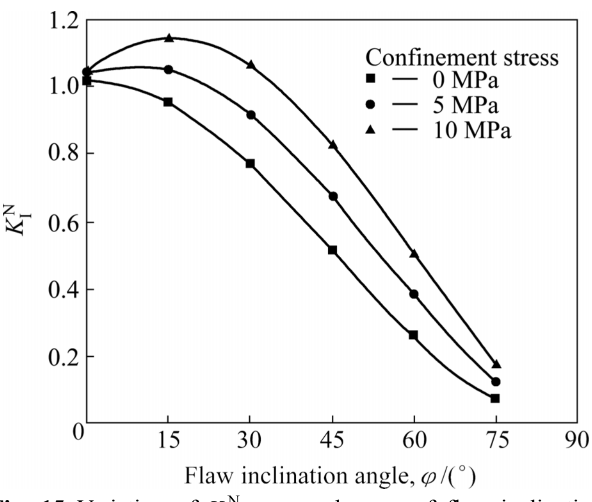

Fig. 15 Variation of K_I^N versus changes of flaw inclination angles (φ) for confinement stress of 0, 5 and 10 MPa

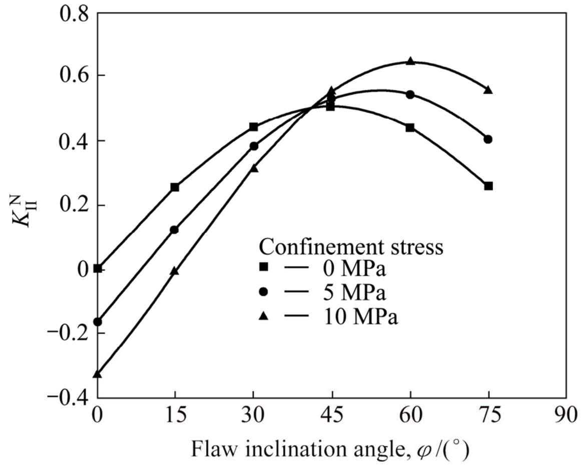

Fig. 16 Variation of K_{II}^N versus changes of flaw inclination angles (φ) for confinement stress of 0, 5 and 10 MPa

4 Discussion

In this work, the cracks propagation path, the cracks coalescence and the effects of confining pressure on the fracturing process of rock and rock-like materials have been studied both experimentally and numerically. The experimental and numerical results given in this work are in good agreement with each other. These results are also comparable with those already cited in Ref. [36]. The following discussion may further augment the validity and accuracy of the present research.

WONG et al [36] have numerically (using a finite element code) presented the solution for the problem shown schematically in Fig. 17 considering a rock-like specimen with length L=170 mm and width w=50 mm (L/w=3.4) containing a center slant flaw with a half-length b=10 mm and inclination angle, φ, changing counterclockwise from x axis.

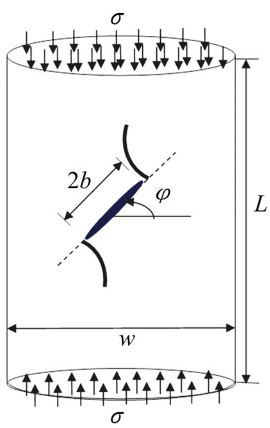

Fig. 17 A schematic view of a propagated center slant flaw (with two wing cracks) in a rock specimen under uniaxial compression

WONG et al [36] have been numerically investigated the crack propagation patterns for different flaw inclination angles, φ= 30°, 45° and 65°. They have used the RFPA^{2D} code (a 2D finite element code) to conduct a number of numerical simulations. Table 3 gives the mechanical properties of rock specimens used in their simulations.

Table 3 Mechanical properties of a rock specimen [36]

Parameter	Value
Flaw length, $2b$/mm	20
Uniaxial compression strength, σ/MPa	200
Elastic modulus, E/GPa	50
Poisson ratio, ν	0.25
Fracture toughness, K_{IC}/(MPa·m$^{1/2}$)	1.2

Figure 18 illustrates the numerical results presented by WONG et al [36] using RFPA^{2D} simulations of the crack propagating patterns in pre-cracked specimens with variable flaw inclination angles, φ=30°, 45°, and 65°, respectively.

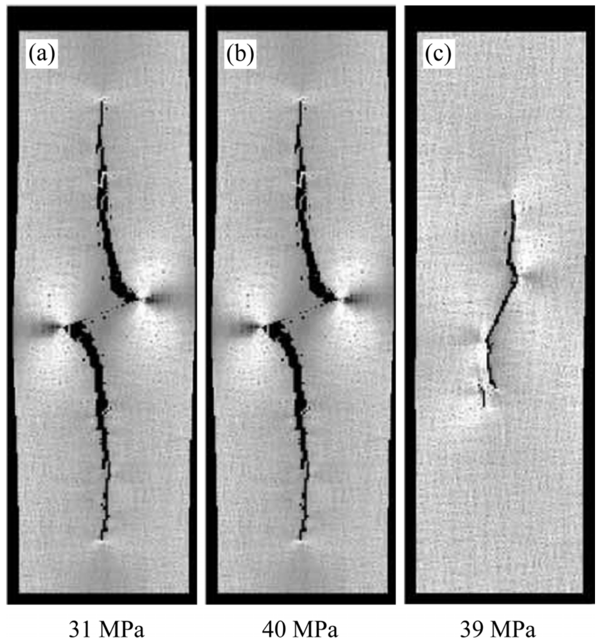

Fig. 18 RFPA^{2D} simulation of propagating paths in pre-cracked specimens with variable flaw inclination angles: (a) φ=30°, (b) φ=45°; (c) φ=65° [36]

In this work, the same problem is solved numerically with the proposed indirect boundary element method. The numerical results obtained by the boundary element simulation of pre-cracked specimens are shown in Fig. 19. Comparing Fig. 18 and Fig. 19 illustrates that the crack propagation paths shown in Fig. 16 are in good agreement with the numerical results given by WONG et al [36] in Fig. 18. Therefore, comparing the results graphically shown in Figs. 18 and 19 clearly demonstrates the accuracy and validity of the boundary element results presented in this work. It should be noted that the boundary element code is much faster and it is quite easy to work with it because the boundary element method essentially reduces one dimension of the problem, alternatively reduces the mesh size sharply and makes the discretization of the problem simpler and quicker [36].

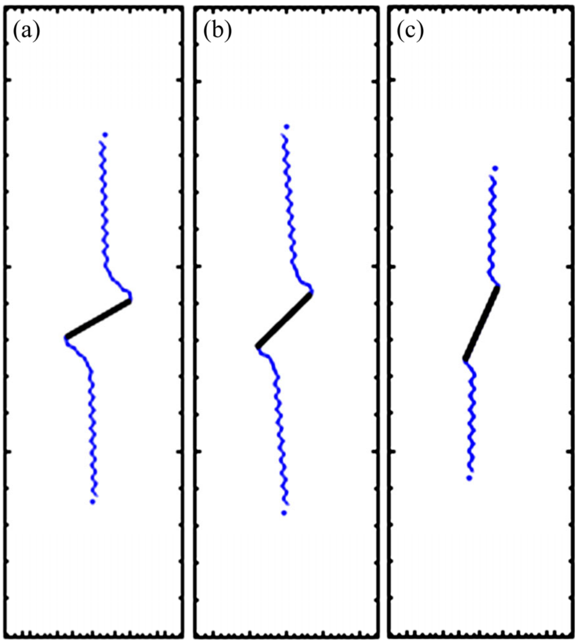

Fig. 19 Boundary element simulation of crack propagation process in pre-cracked specimens (based on mechanical properties given in Table 3): (a) φ=30°; (b) φ=45°; (c) φ=65°

In the numerical verification of the results, the mode I fracture toughness K_{IC}=1.2 MPa·m$^{1/2}$ is estimated based on the numerical results given by WONG et al [36]. It should be noted that different crack propagation increments (steps) are used in the numerical analysis of the present problem.

5 Conclusions

1) A comprehensive experimental works have been accomplished to investigate the crack propagation mechanism in brittle substances due to the cracks coalescence phenomenon which mainly occurs during the propagation of wing cracks emanating from the tips of the pre-existing cracks.

2) It is experimentally shown that the wing cracks are mainly responsible for the cracks coalescence and the final cracks propagating paths. The secondary cracks may also be produced after the propagation of the wing cracks in the specimens under uniaxial loadings. The experimental models illustrate well the production of the wing and secondary cracks and the cracks propagation paths produced by the coalescence phenomenon of the two pre-existing cracks (flaws).

3) The same experimental specimens are modeled numerically by an indirect boundary element method and it has been shown that the numerical results are in good agreement with the corresponding experimental results. The effects of the orientation of the second flaw on the propagation path and cracks coalescence have also been studied experimentally and numerically.

4) The wing cracks initiation stresses for the specimens change from 11.3 to 14.1 MPa in the case of numerical simulations and from 7.3 to 13.8 MPa in the case of experimental works. The cracks coalescence stresses change from 21.8 to 25.3 MPa and from 19.5 to 21.8 MPa in the numerical and experimental analyses, respectively.

5) The effect of confining pressure on the crack propagation process has been numerically simulated, which shows that the SIFs increase and the crack initiation angles change in this case.

References

[1] MILLER J T, EINSTEI H H. Crack coalescence tests on granite [C]// Proceedings of 42nd US Rock Mechanics Symposium. San Francisco, ARMA, 2008: 8−162.

[2] WONG L N Y, EINSTEIN H H. Systematic evaluation of cracking behavior in specimens containing single flaws under uniaxial compression [J]. Int J Rock Mech Min Scie, 2009, 46: 239−249.

[3] YANG S Q. Crack coalescence behavior of brittle sandstone samples containing two coplanar fissures in the process of deformation failure [J]. Engin Fract Mech, 2011, 78: 3059−3081.

[4] HAERI H, SHAHRIAR K, MARJI M F, MOAREFVAND P. On the crack propagation analysis of rock like Brazilian disc specimens containing cracks under compressive line loading, [J]. La Am J Solids and Structures, 2013.

[5] JAEIRO R P, EINSTEIN H H. Experimental study of the cracking behavior of specimens containing inclusions (under uniaxial compression) [J]. Int J Fract, 2010, 164: 83−102.

[6] KE C C, CHEN C S, TU C H. Determination of fracture toughness of anisotropic rocks by boundary element method [J]. Rock Mech Rock Engng, 2008, 41: 509−538.

[7] TANG Chun-an, YANG yue-feng. Crack branching mechanism of rock-like quasi-brittle materials under dynamic stress [J]. Journal of Central South University, 2012, 19: 3273−3284.

[8] ZHAO Yan-lin, CAO Ping, WANG Wei-jun, WAN Wen, CHEN Rui. Wing crack model subjected to high hydraulic pressure and far field stresses and its numerical simulation [J]. Journal of Central South University, 2012, 19: 578−585.

[9] BEHNIA M, GOSHTASBI K, MARJI M F, GOLSHAI A. Numerical simulation of crack propagation in layered formations [J/OL]. Arab J Geosci, 2013, doi: 10.1007/s12517-013-0885-6.

[10] Ghazvinian A, NEJATI HR, SARFARAZI V, HADEI M R. Mixed mode crack propagation in low brittle rock-like materials [J/OL]. Arab J Geosci. 2012, doi: 10.1007/s12517-012-0681-8.

[11] LI H, WONG L N Y. Influence of flaw inclination angle and loading condition on crack initiation and propagation [J]. Int J Solids and Structures, 2012, 49: 2482−2499.

[12] HAERI H, SHAHRIAR K, MARJI M F. MOAREFVAD P. A coupled numerical-experimental study of the breakage process of brittle substances [J/OL]. Arab J Geosci, 2013, doi: 10.1007/s12517-013-1165-1.

[13] BOMBOLAKIS E G. Photoelastic study of initial stages of brittle fracture in compression [J]. Tectonophysics, 1968, 6: 461−473.

[14] JIEFAN H, GANGLIN C, YONGHONG Z, REN W. An experimental study of the strain field development prior to failure of a marble plate under compression [J]. Tectonophysics, 1990, 175: 269−284.

[15] BOBET A. The initiation of secondary cracks in compression [J]. Engineering Fracture Mechanics, 2000, 66: 187−219.

[16] PARK N S. Crack Propagation and coalescence in rock under uniaxial compression. [D]. Seoul: Seoul National University, 2001.

[17] WONG R H C, CHAU K T, TANG C A, LIN P. Analysis of crack coalescence in rock-like materials containing three flaws: Part I. Experimental approach [J]. Int J Rock Mech Min Scie, 2001, 38: 909−924.

[18] SAHOURYEH E, DYSKIN A V, GERMANOVICH L N. Crack growth under biaxial compression [J]. Engin Fract Mech, 2002, 69: 2187−2198.

[19] LI Y P, CHEN L Z, WANG Y H. Experimental research on pre-cracked marble under compression [J]. Int J Solids and Structures, 2005, 42: 2505−2516.

[20] PARK C H, BOBET A. The initiation of slip on frictional fractures. Golden rocks [R]. ARMA/USRMS, 2006: 06−923.

[21] PARK C H, BOBET A. Crack Initiation and propagation from frictional fractures [C]// Proceedings of 1st Canada-US Rock Mechanics Symposium. 2007: 557−564.

[22] WONG L N Y, EINSTEIN H H. Crack coalescence in molded gypsum and Carrara marble: Part 1. Macroscopic observations and interpretation [J]. Rock Mech Rock Engine, 2008, 42: 475−511.

[23] WONG L N Y, EINSTEIN H H. Crack coalescence in molded gypsum and Carrara marble: Part 2. Microscopic observations and interpretation [J]. Rock Mechanics and Rock Engineering, 2008, 42: 513−545.

[24] PARK C H. Coalescence of frictional fractures in rock materials [D]. Indiana, Purdue University West Lafayette, 2008.

[25] PARK C H, BOBET A. Crack coalescence in specimens with open and closed flaws: A comparison [J]. Int J Rock Mech Min Scie, 2009, 46: 819−829C.

[26] YANG Q, DAI Y H, HAN L J, JIN Z Q. Experimental study on mechanical behavior of brittle marble samples containing different flaws under uniaxial compression [J]. Engin Fract Mech, 2009, 76: 1833−1845S.

[27] PARK C H, BOBET A. Crack initiation, propagation and coalescence from frictional flaws in uniaxial compression [J]. Engin Fract Mech, 2010, 77: 2727−2748.

[28] LEE H, JEON S. An experimental and numerical study of fracture coalescence in pre-cracked specimens under uniaxial compression [J]. Int J of Solids and Structures, 2011, 48: 979−999.

[29] PU Cheng-zhi, CAO Ping. Failure characteristics and its influencing factors of rock-like material with multi-fissures under uniaxial compression [J]. Transactions of Nonferrous Metals Society of China, 2012, 22: 185−191.

[30] ERDOGAN F, SIH G C. On the crack extension in plates under loading and transverse shear [J]. J Fluids Eng, 1963, 85: 519−527.

[31] HUSSIAN MA, PU E L, UNDERWOOD J H. Strain energy release rate for a crack under combined mode I and mode II [R]. Fracture Analysis. ASTM STP 560. American Society for Testing and Materials, 1974: 2−28.

[32] SIH G C. Strain–energy–density factor applied to mixed mode crack problems [J]. International Journal of Fracture, 1974, 10: 305−321.

[33] SHEN B, STEPHANSSON O. Modification of the G-criterion for crack propagation subjected to compression [J]. Engin Fract Mech, 1994, 47: 177−189.

[34] MARJI M F, HOSSEIN_NASAB H, KOHSARY A H. On the uses of special crack tip elements in numerical rock fracture mechanics [J]. Int J Solids and Structures, 2006, 43: 1669−1692.

[35] MARJI M F. On the use of power series solution method in the crack analysis of brittle materials by indirect boundary element method [J]. Engin Fract Mech, 2013, 98: 365−382.

[36] WONG R H C, TANG C A, CHAU K T, LIN P. Splitting failure in brittle rocks containing pre-existing flaws under uniaxial compression [J]. Engin Frac Mecha, 2002, 69: 1853−1871.

[37] MANOUCHEHRIAN A, MARJI M F. Numerical analysis of confinement effect on crack propagation mechanism from a flaw in a pre-cracked rock under compression [J]. Acta Mechanica Sinica, 2012, 28: 1389−1397.

[38] CROUCH S L. Analysis of stresses and displacements around underground excavations: An application of the Displacement Discontinuity Method. University of Minnesota Geomechanics Report [R]. Minneapolis, Minnesota, 1967.

[39] GUO H, AZIZ N I, SCHMIDT R A. Linear elastic crack tip modeling by displacement discontinuity method [J]. Engin Fract Mech, 1990, 36: 933−943.

[40] SCAVIA C. Fracture mechanics approach to stability analysis of crack slopes [J]. Engng Fract Mech, 1990, 35: 889−910.

[41] ALIABADI M H, ROOKE D P. Numerical Fracture Mechanics [M]. Southampton, U.K., Computational Mechanics Publications, 1991.

[42] BEHNIA M, GOSHTASBI K, MARJI M F, GOLSHANI A. On the crack propagation modeling of hydraulic fracturing by a hybridized displacement discontinuity/boundary collocation method [J]. J Min and Enviro, 2011, 2: 1−16

[43] HAERI H, SHAHRIAR K, MARJI M F, MOAREFVAND P. Modeling the propagation mechanism of two random micro cracks in rock samples under uniform tensile loading [C]// Proceedings of 13th International Conference on Fracture. Beijing, China, 2013.

[44] HAERI H, AHRANJANI K A. A fuzzy logic model to predict crack propagation angle under disc cutters of TBM [J]. Int J Academic Research, 2012, 4: 159−169.

[45] CROUCH S L, STARFIELD A M. Boundary element methods in solid mechanics [M]. London, Allen and Unwin, 1983.

[46] WHITTAKER, B N, SINGH R N, SUN Q. Rock fracture mechanics, principals, design and applications, developments in geotechnical engineering [R]. Amsterdam, Elsevier, 1992.

[47] ALIABADI M H. Fracture of rocks [M]. Southampton, U.K.: Computational Mechanics Publications, 1998.

[48] SHOU K J, CROUCH S L. A higher order displacement discontinuity method for analysis of crack problems [J]. Int J Rock Mech Min Sci and Geomech, Abstr, 1995, 32: 49−55.

[49] HAERI H. Numerical modeling of the interaction between micro and macro cracks in the rock fracture mechanism using displacement discontinuity method [D]. Department of Mining Engineering, Science and Research Branch, Islamic Azad University, Tehran, Iran, 2013.

[50] IRWIN G R. Analysis of stress and strains near the end of a crack [J]. J Appl Mech, 1957, 24: 361−364.

[51] MARJI M F, DEHGHAI I. Kinked crack analysis by a hybridized boundary element/boundary collocation method [J]. Int J Solids and Structures, 2010, 47: 922−933.

(Edited by YANG Bing)